A molecular perspective for global modeling of upper atmospheric NH_3 from freezing clouds

Cui Ge[a,1], Chongqin Zhu[b,1], Joseph S. Francisco[b,2], Xiao Cheng Zeng[b,2], and Jun Wang[a,2]

[a]Department of Chemical and Biochemical Engineering, The University of Iowa, Iowa City, IA 52242; and [b]Department of Chemistry, University of Nebraska–Lincoln, Lincoln, NE 68588

Contributed by Joseph S. Francisco, May 7, 2018 (sent for review November 15, 2017; reviewed by Lyatt Jaegle and Jingqiu Mao)

Ammonia plays a key role in the neutralization of atmospheric acids such as sulfate and nitrates. A few in situ observations have supported the theory that gas-phase NH_3 concentrations should decrease sharply with altitude and be extremely low in the upper troposphere and lower stratosphere (UTLS). This theory, however, seems inconsistent with recent satellite measurements and is also not supported by the aircraft data showing highly or fully neutralized sulfate aerosol particles by ammonium in the UTLS in many parts of the world. Here we reveal the contributions of deep convective clouds to NH_3 in the UTLS by using integrated cross-scale modeling, which includes molecular dynamic simulations, a global chemistry transport model, and satellite and aircraft measurements. We show that the NH_3 dissolved in liquid cloud droplets is prone to being released into the UTLS upon freezing during deep convection. Because NH_3 emission is not regulated in most countries and its future increase is likely persistent from agricultural growth and the warmer climate, the effect of NH_3 on composition and phase of aerosol particles in the UTLS can be significant, which in turn can affect cirrus cloud formation, radiation, and the budgets of NOx and O_3.

ammonia | molecular dynamics simulation | global model | deep convection | freezing clouds

Ammonia, the most abundant gas-phase alkaline species in the atmosphere, contributes considerably to the neutralization of atmospheric acids produced by the oxidation of sulfur and nitrogen oxidizes with major anthropogenic sources (1, 2). NH_3 mainly comes from fertilizers and animals, and other sources include industry, fossil fuels, oceans, crops, soils, and biomass burning (3, 4). Primarily emitted from land surfaces, ammonia has a lifetime of several hours due to its high affinity to water, which facilitates its effective removal via atmospheric scavenging and its incorporation in aqueous and acid particles (1, 2). Hence, gas-phase NH_3 concentrations are expected to decrease sharply with altitude and to be extremely low in the upper troposphere and lower stratosphere (UTLS), especially over the ocean (1, 5–7). This expectation is supported by several in situ observations (1, 5–7). However, in situ measurements of NH_3, a sticky, semivolatile compound with ambient concentrations that vary by several orders of magnitude, may have large uncertainties in the UTLS (8). Recent satellite measurements give different insights and show significant amounts of NH_3 (above 15 pptv) in the UTLS over the subtropical regions of the southeastern Asian continent (20–30°N, 70–110°E) during the summer monsoon season (9). Furthermore, although NH_3 and NH_4^+ in the UTLS are widely thought to be in extremely low concentrations, the aircraft data showed the relative high ratio of $[NH_4^+]/(2 \times [SO_4^{2-}])$ in the UTLS in many parts of the world, including over the remote southern Pacific Ocean (10, 11). To solve the puzzle concerning the missing source of NH_3 in the UTLS, we utilize a cross-scale modeling approach that includes molecular dynamic (MD) simulations and a global chemistry transport model. We show that the NH_3 dissolved in liquid cloud droplets is released into the UTLS upon freezing and that there is a subsequent collision of ice particles during deep convection, thereby explaining the unexpectedly high concentrations of NH_3 in many parts of the world.

Tropical deep convection is a critical mechanism for the transfer of surface air masses and insoluble trace gases (such as CO) from the lower to the upper atmosphere with many important implications for atmospheric chemistry (12, 13). Liu and Zipser (14) found that the deepest convection was located over South America and Africa. Penetration of these trace gases to high altitudes (16–18 km) has also been observed in northern Australia (15, 16) and over tropical cyclones (10, 17, 18). Southeast Asia is one of the tropical regions with frequent deep convection associated with the Asian summer monsoon anticyclone (19). Major source regions of NH_3 are located in southeast China and northern India (9, 20, 21). Very few measurements of NH_3 have been made in the middle and upper atmosphere (9). Before 2008, measurements of ammonia were almost exclusively based on in situ technologies, and most of them focused on ground-level concentrations with few observations above the boundary layer (22). By contrast, satellite measurements of infrared spectra have been used in the past decade to derive the amounts of NH_3 in the atmosphere (3, 23–27), and limb-sounding techniques have been proposed to measure the vertically resolved profiles of NH_3 in the UTLS (28–30). Before 2016, no data from in situ measurements and limb-sounding remote-sensing data (9) showed ammonia to be present at altitudes above 8 km. Höpfner et al. (9) presented the first evidence of the presence of ammonia in the UTLS

Significance

The retentions of gases upon freezing of water from available studies are conflicting. Using molecular dynamic simulations, we have revealed that the retention efficiency of NH_3 upon freezing cloud is close to 0 rather than 1 during deep convection. Our results further provide theoretical framework to explain the first-ever satellite-observed high concentration of NH_3 in the upper troposphere and lower stratosphere (UTLS). As NH_3 emission continues to increase, this study calls upon the emergent need to assess the role of NH_3 in UTLS chemistry especially in the deep convective regions. Methodologically, the molecular dynamics simulation is demonstrated as a tool for improving parameterization of interactions between trace gases and cloud (including ice) particles in global atmospheric models.

Author contributions: C.G., C.Z., J.S.F., X.C.Z., and J.W. designed research; C.G., C.Z., and J.S.F. performed research; J.S.F., X.C.Z., and J.W. contributed new reagents/analytic tools; C.G., C.Z., J.S.F., X.C.Z., and J.W. analyzed data; and C.G., C.Z., J.S.F., X.C.Z., and J.W. wrote the paper.

Reviewers: L.J., University of Washington; and J.M., University of Alaska Fairbanks.

The authors declare no conflict of interest.

[1]C.G. and C.Z. contributed equally to this work.

[2]To whom correspondence may be addressed. Email: jfrancisco3@unl.edu, xzeng1@unl.edu, or jun-wang-1@uiowa.edu.

This article contains supporting information online at www.pnas.org/lookup/suppl/doi:10.1073/pnas.1719949115/-/DCSupplemental.

Published online May 30, 2018.

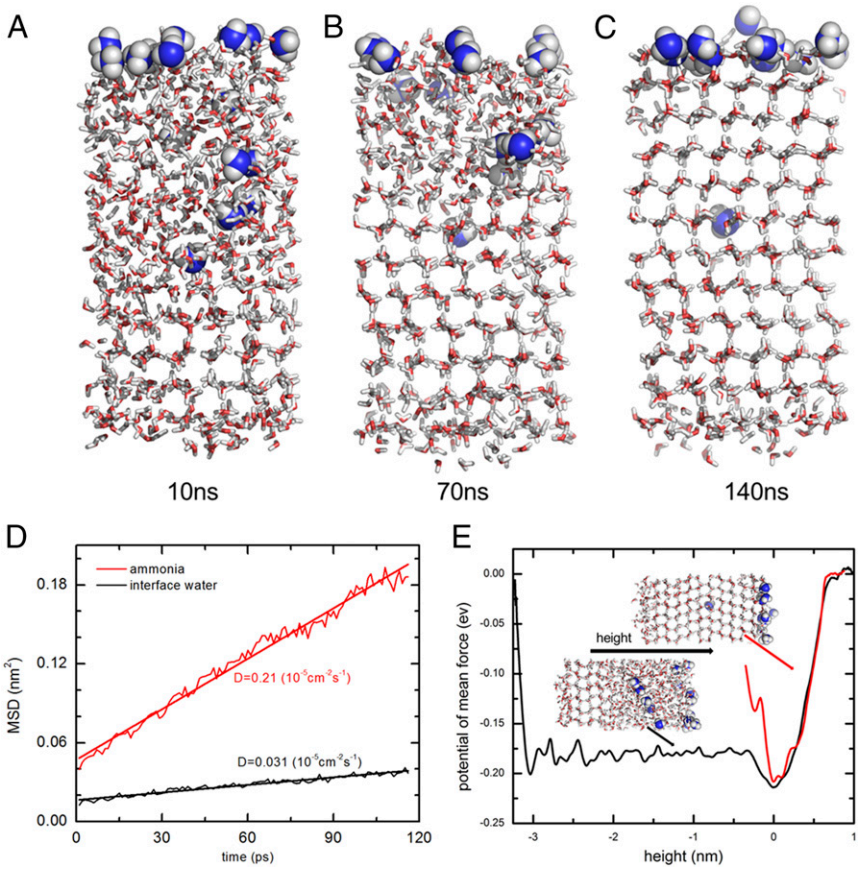

Fig. 1. MD simulations of ice growth with NH_3 initially dissolved in the liquid layer. Snapshots from the MD simulation. (*A*) 10 ns, (*B*) 70 ns, and (*C*) 140 ns. N and H are denoted by the blue and white spheres, respectively. (*D*) The computed MSDs of the water molecules and ammonia molecules in the liquid layer versus time. The starting/zero point of the time axis is set at 140 ns in the MD simulations. The self-diffusion constant of the interface water at 200 K ($D = 0.031 \times 10^{-5}$ cm^2/s) is considerably higher than that of the bulk ice whose diffusion constant is typically on the order of 10^{-9} cm^2/s. This confirms the presence of liquid phase at the interface. Because of the high mobility of the interface water, the self-diffusion constant for the ammonia ($D = 0.21 \times 10^{-5}$ cm^2/s) at the interface is also very high, which will facilitate the evaporation of ammonia molecules. (*E*) The computed PMF of the ammonia molecule from the ice–water interface, passing through the liquid layer, to the air–liquid interface at (*A*) 10 ns (black line) and (*B*) 140 ns (red line). For 10 ns, two local minima are placed at the ice–water interface (−0.2 eV) and at the air–water interface (−0.22 eV). For 140 ns, only one minimum is observed suggesting ammonia molecules prefer to stay at the air interface.

above 10 km over the Asian summer monsoon system and compared against several global modeling results with either low horizontal resolutions (in range of ∼5–10°) or low vertical resolutions (with total number of vertical layers ranging from 9 to 26). Höpfner et al. (9) concluded that no literature regarding locally resolved model results of NH_3 during the monsoon period over Asia is available to compare with their novel observations.

The scavenging of NH_3 by monsoon convection is hypothesized to incompletely deplete atmospheric NH_3, thereby leading to the direct transport of NH_3 from the boundary layer to the UTLS via convection (9). Our study seeks another pathway for the vertical transport of NH_3 via the interactions between NH_3 and clouds. Ammonia gas has a large proton affinity and can therefore serve as a base to neutralize liquid particles (either aerosols or cloud droplets) that are often weakly acidic. The ammonia gas can dissolve in the liquid cloud. During the upward movements driven by deep convection, the liquid droplets of clouds are first supercooled and then frozen in the UTLS before they precipitate with atmospheric downdrafts. During this process of liquid-to-ice conversion, some gases in the liquid cloud droplets might be trapped inside the ice particles, but other trace gases might be released into the atmosphere upon freezing; the relative amount of the gas that is retained in this conversion process is characterized by the retention coefficient of that gas (31). Past studies have derived the retention coefficients of different gas species through several laboratory experiments, aircraft measurements, and theoretical calculations but showed controversial results. SO_2 is one of the most studied species, and its retention coefficients vary from 0.02 (13, 32), to 0.03–0.14 (33) to 0.25–0.9 (34, 35). For H_2O_2, the retention coefficient is reported as being between 0.64 (31) and 1 (34). As a highly soluble trace gas, HNO_3 has been reported close to 1 (31, 36). The retention coefficients of some other species have also been reported: 1 for H_2SO_4 (36); 0 for O_3, NO, NO_2, NO_3, N_2O_5, and CO_2; 0.02 for OH, CH_3O_2, and CH_3OOH; and 0.65 for HO_2, HNO_2, HNO_4, HCHO, HCOOH, and CH_3COOH (37). These studies show that the direct measurement of retention efficiency can be affected by other factors in the laboratory and/or ambient environment, including temperature, strength of dissociation, wet/dry ice cloud growth conditions, riming intensity, concentrations, drop sizes, air speeds, ventilation, etc. (13, 31, 32, 37, 38). Indeed, for NH_3, the retention coefficients reported in the literature fall within wide ranges, such as <0.01 (39), 0.29–1 (31), and 1 (32).

In the numerical simulations of the interactions between atmospheric chemistry and freezing clouds, retention is the main process that decides the in-cloud scavenging of trace gases by cloud ice particles (40). Salzmann et al. (41) conducted simulations that assumed that H_2O_2 was either completely released or completely retained during freezing because H_2O_2 retention coefficients of 0 and 1 were both reported (35, 42). They concluded that the inefficient scavenging of H_2O_2 by the ice in clouds of tropical storms in combination with an upper air chemical source can contribute to the observed increases of the mixing ratios of H_2O_2 in deep convective outflows. Michael and Stuart (43) calculated the retentions of six trace chemicals, SO_2, H_2O_2, NH_3, HNO_3, CH_2O, and HCOOH, and found that the overall ranges of the simulated retention fractions were between 1×10^{-8} and 1 in different scenarios. Further, these authors proposed using dynamic retention calculations to represent the changing regimes of cloud models. Ervens (44) emphasized that the removal rates of ice and precipitation are still the most uncertain processes in cloud models due to the uncertainties associated with droplets freezing and the retention of molecule species (40). Several chemistry transport models either do not consider this retention process for NH_3 or treat NH_3 as being completely scavenged (2).

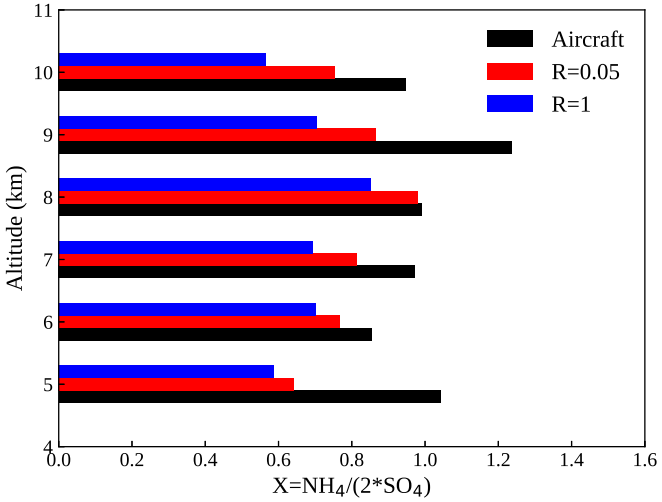

Fig. 2. Vertical profile comparisons between the measured $[NH_4^+]/[2 \times SO_4^{2-}]$ and the GEOS-Chem simulated counterparts. Measured data are the averages of measurements from seven global aircraft campaigns in the years of 1991–2006 to represent the climatology. The simulation data are from the year of 2005 and are sampled along the aircraft tracks.

Results and Discussion

MD Modeling. Herein, we present MD simulations to gain molecular-level insights into the behavior of ammonia in supercooled water during ice growth (*SI Appendix*, Fig. S1). Our focus is mainly on the molecular processes occurring between NH_3 and air–water–ice interface(s). Such a simple scenario is especially true in the regions with high NH_3 sources. To model this scenario using the MD simulation, we placed 16 ammonia molecules in the liquid water slab (containing 409 water molecules) to mimic the very high initial concentrations of ammonia. Our subsequent MD simulation results show that there is no evaporation of ammonia molecules during the individual ice particle growth process (*SI Appendix*, Fig. S2 and Movie S1). Within this period, the ammonia molecules are pushed to the air–liquid interface concurrently with the continued growth of the ice crystals (Fig. 1 *A*–*C* and *SI Appendix*, Fig. S2). According to our simulations, after the ice growth stops and the ice crystallization reaches the air–liquid interface, only 3 out of 16 ammonia molecules are evaporated within a very short period (*SI Appendix*, Fig. S2). However, no additional ammonia evaporation events are observed as the system reaches an equilibrium state. Other simulations are also conducted for a total of 6, 8, 10, or 12 ammonia molecules in the supercooled water droplets, respectively. All MD simulations demonstrate that the surface air–water layer can accommodate 94–100% ammonia molecules, a feature consistent with several laboratory measurements (31, 32). In other words, in realistic atmospheric situations (such as winter stable cloud condition) where the ammonia concentrations are orders of magnitude lower than those used in the MD simulation, the ammonia molecules trapped in the surface air–water layer of the ice particles cannot be easily evaporated under nonconvective conditions.

Furthermore, the computed mean square displacements (MSDs) of the water and ammonia molecules at the interface suggest that the ice core is wet by a thin liquid-like layer (Fig. 1*D*). In addition, to quantitatively measure the tendencies of the ammonia evaporation from the ice particle, the free-energy barrier of the ammonia evaporation is estimated (Fig. 1*E*). To this end, we computed the free-energy profile of an ammonia molecule moving from the ice–water interface, passing through the liquid water layer, toward the air–liquid interface. Before the ice growth, the ammonia molecules located at the air–liquid interface can either diffuse into the liquid water layer or out into the air. Due to the much lower energy barrier (0.04 eV) of the liquid layer, ammonia molecules at the air–liquid interface tend to diffuse into the liquid layer rather than into the air, explaining why no ammonia evaporation is observed before and during the ice growth. Once the entire liquid layer turns into ice, only a single free-energy minimum is observed (red line in Fig. 1), suggesting that the ammonia molecule tends to be located at the air interface rather than being trapped inside the ice phase. This behavior is further confirmed by the snapshots shown in Fig. 1*C* and *SI Appendix*, Movie S2. Hence, once the ice growth ceases, the ammonia molecules located at the thin air–liquid interface can only diffuse into the air and cannot move into the ice phase.

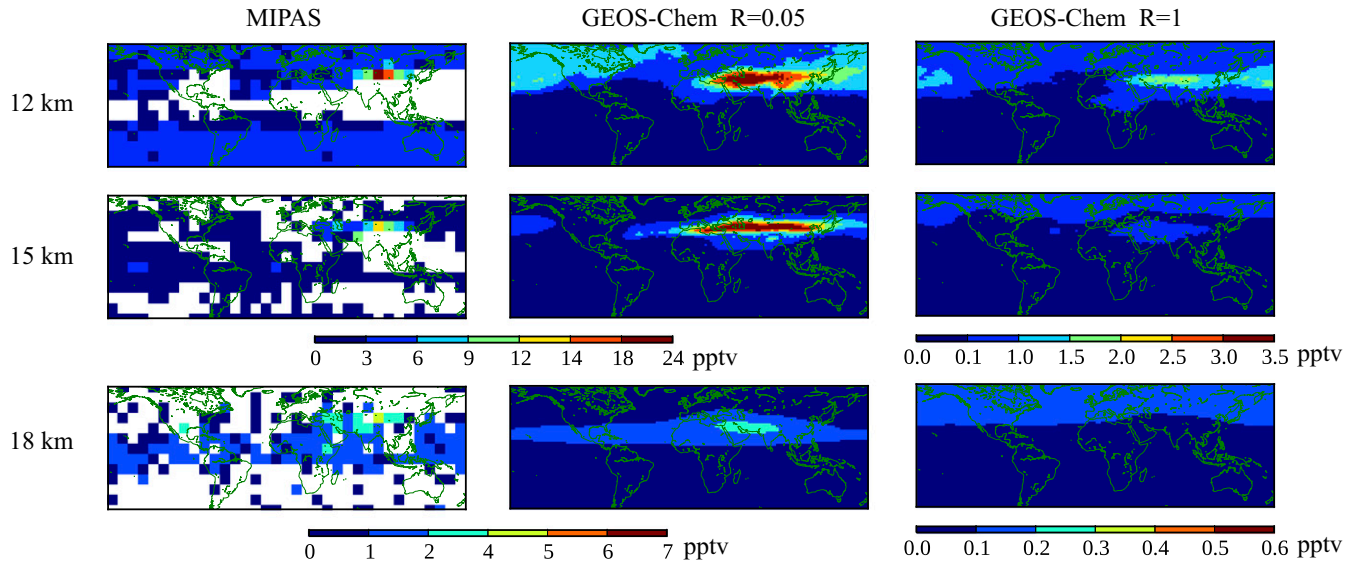

Fig. 3. Comparing the simulations with the satellite-measured seasonal averaged (June, July, and August) NH_3 values at (*Top*) 12 km, (*Middle*) 15 km, and (*Bottom*) 18 km over Asia. The modeled NH_3 shows the 6 y average (2003 and 2007–2011) and from the R1 and R0.05 simulations. The MIPAS-measured NH_3 values are averaged and shown only for grid boxes with more than 4 y valid data.

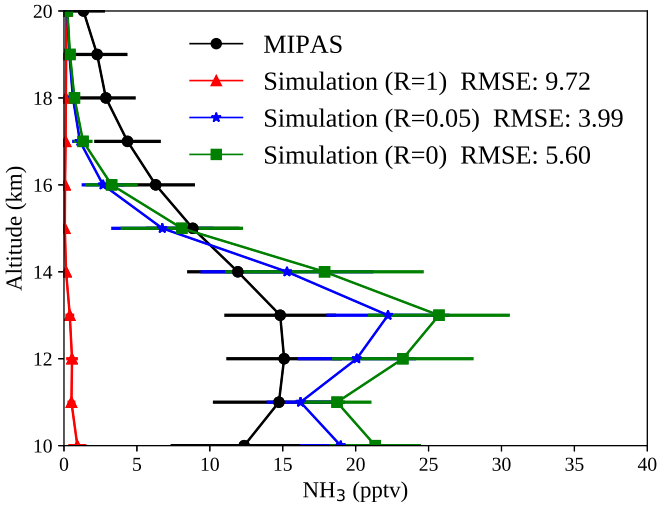

Fig. 4. Comparing the simulations with MIPAS-measured seasonal (June, July, and August) vertical profile of NH_3 over Asia over 6 y (2003 and 2007–2011). The profile of NH_3 volume mixing ratio is averaged over the eastern part of the Asian monsoon area (30–40°N, 70–110°E). The NH_3 simulations are from the R1, R0.05, and R0 modeling results. The SDs are shown as error bars, and also shown are root mean squared error (RMSE).

The Ratio of $[NH_4^+]/(2 \times [SO_4^{2-}])$. To understand the effect of the retention efficiency of NH_3 on the global UTLS $[NH_4^+]/(2 \times [SO_4^{2-}])$ ratio, we performed two GEOS-Chem (Goddard Earth Observing System - Chemistry model) simulations with retention efficiencies of 0.05 and 1, which are referred to as the R0.05 and R1 simulations, respectively. According to MD simulation, during the growth of ice crystals, the ammonia molecules are pushed to the thin air–liquid interface and can only diffuse into the air and cannot move into the ice phase. In deep convective clouds instead of stable wintertime cloud conditions, the air–liquid interface is unlikely to remain (13). So the high mobility of ammonia at the interface and the low free-energy barrier to ammonia evaporation calculated by the MD model indicate that the ammonia molecules are very unstable and prone to evaporation after the collision of ice particles within deep convection. Here 0.05 is selected as a representative for low retention efficiency value. The details of GEOS-Chem can be found in *Materials and Methods* and in *SI Appendix*. The retention efficiency of NH_3 is standardized at 1 in most global chemical transport models (CTMs; 2). GEOS-Chem assumes the retention efficiency of NH_3 as 0.05 (11, 45), which is in line with the evidence from our MD simulations. The sulfate–ammonium particle compositions are characterized by X: $[NH_4^+]/(2 \times [SO_4^{2-}])$. Fig. 2 shows the vertical profile comparisons between the measured and the GEOS-Chem simulated X. The measurement data are from seven aircraft campaigns from 1991 to 2006 and represent the global climate average (*Materials and Methods* and *SI Appendix*, Table S1). The GEOS-Chem simulation data are for 2005 and were sampled along the aircraft tracks. We focus on the differences between the R1 and R0.05 simulations rather than on quantitative comparisons with the observations. The effect of retention occurs mainly at the freezing cloud level of the UTLS, and the aircraft observation altitudes are mostly below 10 km. Thus, Fig. 2 shows X between 5 and 10 km altitudes. Overall, the X values from the R0.05 simulations are greater than that from the simulation of R1, with a difference of up to 0.2. On average, the consideration of NH_3 retention efficiency as 0.05 led to modeled X closer to the observation (1.01) by 0.12 (from 0.68 to 0.80), which reflects the contribution of NH_3 from freezing clouds.

High Concentration of NH_3 over Asia. To interpret Höpfner's (9) satellite observation, we conduct the simulations with and without considering the new pathway for UTLS NH_3 through ice cloud formation. Fig. 3 shows the distribution of the NH_3 volume mixing ratios at altitudes of 12, 15, and 18 km, which is in the range of upper troposphere and lower stratosphere (UTLS) over the subtropical region that has the tropopause in average of 12–13 km in summer (*SI Appendix*, Fig. S7). The modeled seasonal (June, July, and August) NH_3 is the average for 6 y (2003 and 2007–2011) from the R1 and R0.05 simulations, respectively. The satellite-observed seasonal NH_3 values are from Michelson Interferometer for Passive Atmospheric Sounding (MIPAS) (9) and are averaged for only for grid boxes with more than 4 y valid data. MIPAS showed that the enhancement of NH_3 over the Asian monsoon region is prominent at both 12 and 15 km altitudes with ~10 pptv against the global background of <5 pptv. The simulations of both R1 and R0.05 show (Fig. 3) the relative enhancement of NH_3 over the Asian monsoon region. Only the R0.05 simulation is comparable with the MIPAS observations, with values larger than 12 pptv at both 12 and 15 km altitudes. The simulation from R1 shows a very low enhancement of NH_3, with maximum values of up to 1.6 pptv at an altitude of 12 km and up to 0.64 pptv at an altitude of 15 km, both of which are a factor of 6–10 lower than the observed counterparts. The same findings hold for the results at an altitude of 18 km.

The retention efficiency of NH_3 may vary in different altitudes and in different specific cases depending on the efficacy of breaking up the air–water interface of the ice particles in the convective updrafts. To consider this variation, simulations with R value of 0 are conducted. By sampling model results to match the valid MIPAS values for each year and each grid box, the profile of the NH_3 volume mixing ratios is averaged within the eastern part of the Asian monsoon area (30–40°N, 70–110°E) and compared with the MIPAS observed profile (Fig. 4). The performance of R0 is similar to that of R0.05, with slightly better (worse) performance above (below) 15 km altitude (Fig. 4). In contrast, the performance of simulation with $R = 1$ overall is poorer than that of R0.05. The profile of the MIPAS NH_3 revealed that the maximum concentrations of NH_3 in the Asian monsoon area reached ~15 pptv at an altitude of 11–13 km. The R0.05 simulation reproduces this feature with averaged NH_3 of 20 pptv at the same altitude range, whereas the R1 simulation shows less than 2 pptv from the altitude of 10 to 15 km. Statistically,

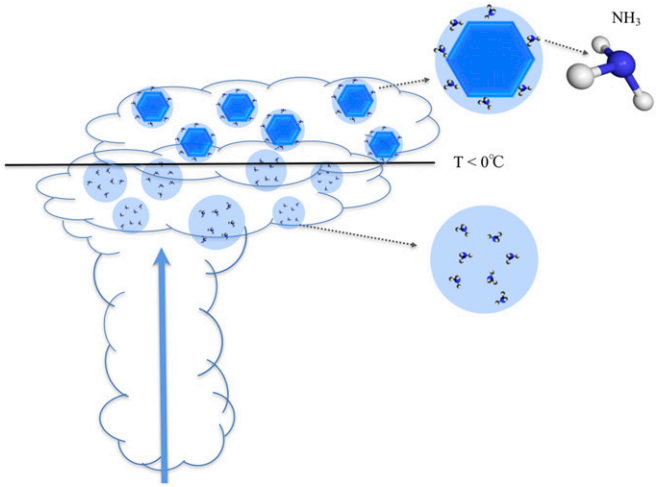

Fig. 5. A schematic of a new pathway for NH_3 in upper atmosphere. NH_3 dissolved in the liquid water cloud droplets is prone to release in the upper atmosphere upon freezing (of ice crystals) during deep convection.

the results with lower retention efficiency are robust. The averaged NH_3 value for 10–20 km altitude is 0.29 pptv (R1), 9.50 pptv (R0.05), and 10.99 pptv (R0) versus the observed value of 8.63 pptv. Further comparison (*SI Appendix*, Fig. S4) with satellite-measured NH_3 at 12, 15, and 18 km over Asian area (30–40°N, 70–110°E) is made for simulations with $R = 0.05$, and the modeled NH_3 is sampled to pair with the valid MIPAS NH_3 data for each summer and each grid box. Only the grid boxes with valid data for at least 4 y are considered here. The correlation between multisummer mean measurements and simulation ($R = 0.05$) is 0.86. The averaged NH_3 is 8.75 pptv from MIPAS and 8.77 pptv from the simulation ($R = 0.05$); both values are above the MIPAS detection limit (3–5 pptv), and their difference is within the error (near and below 1 pptv) of MIPAS retrievals (9). The year to year variations (error bars in *SI Appendix*, Fig. S4) from both MIPAS and the simulation could be up to 10 pptv that may in part reflects interannual changes of summer convection and meteorology.

During nonsummer seasons, we do not find any enhancement of NH_3 over Asia (not shown) from both the simulation and MIPAS measurement values, which indicates that both high NH_3 emissions and frequent deep convection events are two integral parts for the presence of NH_3 in UTLS. Hence, the differences between observed and simulated NH_3 in UTLS can be partly attributed to emission uncertainties and partially to uncertainty in convection in the model. Although few studies have investigated NH_3 emission over India, NH_3 emission inventory of Streets et al. (46), as used in this study, shows a strong peak in June over East Asia including India. In contrast, Huang et al. (47) suggest a weak summer peak of NH_3 emissions in China, whereas the Magnitude and Seasonality of Agricultural Emissions (MASAGE) inventory (20) indicates largest emissions in April and July. The bottom-up NH_3 emissions like Street et al. (46) inventory are estimated ∼15% higher than the top-down estimates in May and June and ∼20% lower in other months. Nevertheless, our model simulations show a large NH_3 emission in Indian summer boundary layer (11), which suggests the possible presence of NH_3 gas in the cloud droplets. Assuming that the NH_3 emission is underestimated by 100%, the simulated UTLS NH_3 concentration for R1 would be increased by a factor of 2 only, which is still lower than MIPAS measurements by at least a factor of 10. Regarding the uncertainties from deep convection in the model, Huang et al. (48) showed GEOS-Chem simulations of CO spatial distributions in UTLS agree well with the satellite observation at 215 and 147 hPa but are underestimated by ∼40% at 100 hPa. Similar to Huang et al.'s (48) finding, our simulated NH_3 is also lower than MIPAS measurements above 15 km by about 50% on average. This uncertainty caused by convection contributes the discrepancy between R0.05 simulation and the observation above 15 km, although it cannot explain the difference of NH_3 between R1 simulation and MIPAS observations in 10–15 km.

The wet scavenging process in the GEOS-Chem model could be another reason to cause uncertainties in the gas or aerosol contents in the UTLS (49), which allows for greater NH_3 survival in the uplift and decreasing the amount of NH_3 lost due to precipitation. We tested the response of NH_3 to wet scavenging efficiency by reducing the wet deposition by 10% (the average range of relative uncertainty in wet deposition in GEOS-Chem) (50) and compared the results from the simulations with wet deposition unchanged. Both simulations had an R value of 1. As expected, more NH_3 is lifted to 12 and 15 km in the simulation with 90% wet deposition than in the simulations with 100% wet deposition (Fig. 3 and *SI Appendix*, Fig. S5); however, the NH_3 values still remained much lower than those of the MIPAS observations. For example, at an altitude of 12 km, the high value of the NH_3 mixing ratio over the Asian monsoon area is ∼4 pptv with 90% wet deposition and is ∼1.6 pptv with wet deposition unchanged. Both the MIPAS and R0.05 simulations with wet deposition unchanged have NH_3 of 10 pptv and larger. In summary, direct transport of NH_3 during deep convection has a minor contribution to high concentration of NH_3 in UTLS. If we consider doubling NH_3 emissions, it could increase NH_3 at 12 km from 1.6 to 3.2 pptv. Decreasing wet scavenging to 90% increases NH_3 at 12 km from 1.6 to 4.0 pptv (*SI Appendix*, Fig. S5). Hence, consideration of combined uncertainties in NH_3 emission and wet scavenging could result in the maximum value of NH_3 of 5.6 pptv, which is still less than 10 pptv as shown in the MIPAS measurements and R0.05 simulations. Among the uncertainties addressed above, although there is a possibility for NH_3 (gas) to survive in the wet scavenging and to be uplifted to UTLS, the low retention effects of NH_3 in ice clouds over the Asian monsoon region are a dominant (albeit not exclusive) contributor to the high NH_3 concentrations over the Asian monsoon region. This result is further supported by the observation of the homogeneous freezing of supercooled water droplets at temperature of 235.15 K or lower in the case of strong updrafts (51), due to shorter transit times that allow the liquid drops to reach high altitudes (51, 52). Hence, the conversion from liquid to ice cloud particles can occur in UTLS during deep convection conditions over Asia where air temperature at tropopause (∼12 km) is on average ∼226 K (*SI Appendix*, Fig. S7).

Summary and Discussion

The presence of NH_3 in the UTLS suggests that stratospheric aerosol particles are not ubiquitously 75% sulfate acid as often believed (53) or assumed in the global models for climate prediction (54), and their composition can be in the form of ammonium sulfate and ammonium nitrate, at least over Asia in summer. Indeed, ammonium sulfate in stratospheric aerosols (up to 28 km) was reported by Bigg (55) over Wyoming, United States, and by Gras (56) over Mildura, Australia. Overall, the summary of early in situ data by Turco et al. (57) estimated that $(NH_4)_2SO_4$ may weigh 10% in total stratospheric aerosol mass but admitted that the presence of ammonia in UTLS is "an open question." This study reveals the importance of release of NH_3 from freezing clouds (as summarized in Fig. 5) in the deep convective systems for the presence of NH_3 in the UTLS by integrating MD modeling, global transport modeling, and limited satellite measurements. Although our analysis focuses on NH_3 over the western Asian summer monsoon region, this pathway for UTLS NH_3 also has implications for other trace gases and locations. Many regions are affected by gas pollution that encounters deep convection systems, such as North America, tropical Africa, and Australia. For example, the simulation shows (*SI Appendix*, Fig. S6) the enhancement of NH_3 concentrations over tropical Africa during the boreal winter season at 12 km in our R0.05 simulations but not in the R1 simulations. Furthermore, in UTLS where relative humidity (with respect to liquid water) is low, ammonium sulfate is more likely in the solid phase, which may facilitate the formation of cirrus clouds (58) and affect the Earth's radiative energy budget (45). The presence of NH_3 can also lead to formation of nitrate aerosols through its reaction with nitric acid, which can in turn affect NOx-catalyzed mechanism for O_3 loss in the stratosphere. Therefore, explicit consideration of role of NH_3 in both chemistry transport and climate models is emergently important, especially after considering that NH_3 emission continues to grow in part due to the increased use of fertilization in agriculture (3, 4) and in part due to nonexistence of policy to regulate NH_3 emissions in many parts of the world. Such advancement in earth system models can be carried out and evaluated with more observation data of trace gases and (aerosol and cloud) particle composition in UTLS and through the adoption of MD simulation as a tool for improving parameterization of interactions between trace gases and particles at air–particle interface.

Materials and Methods

MD Simulation. The MD simulations are carried out using the Groningen Machine for Chemical Simulations 4.5 program. More detailed methods and models are given in *SI Appendix*.

Global Chemical Transport Model. A global 3D CTM, GEOS-Chem (59), is used to simulate the transport, deposition, oxidation, and other related chemical processes of trace gases and aerosols. More detailed model is given in *SI Appendix*.

Aircraft Measurements. Aircraft measurements of the NH_4^+ and SO_4^{2-} from seven field campaigns are analyzed in this study. More detailed information is given in *SI Appendix*.

Satellite NH_3 Data. The seasonal (3-monthly) NH_3 averages within the bins of 10° latitude by 10° longitude and a 1-km altitude are provided at www.imk-asf.kit.edu/english/308.php by Höpfner et al. (9). More detailed information is given in *SI Appendix*.

ACKNOWLEDGMENTS. J.W. is supported by grants from NASA (Grants NNX17AF77G and NNX17AF63G). J.S.F. and X.C.Z. are supported by the NSF (Grant CHE-1665325). The Holland Computing Center of the University of Nebraska, which receives support from the Nebraska Research Initiative, and the High Computing Center in the University of Iowa, which receives support from the University of Iowa's Informatics Initiative, are both acknowledged for their computational support for this work.

1. Dentener F, Crutzen PJ (1994) A three-dimensional model of the global ammonia cycle. *J Atmos Chem* 19:331–369.
2. Adams P, Seinfeld JH, Koch DM (1999) Global concentrations of tropospheric sulfate, nitrate, and ammonium aerosol simulated in a general circulation model. *J Geophys Res* 104:13791–13823.
3. Warner JX, Wei Z, Strow LL, Dickerson RR, Nowak JB (2016) The global tropospheric ammonia distribution as seen in the 13-year AIRS measurement record. *Atmos Chem Phys* 16:5467–5479.
4. Warner JX, et al. (2017) Increased atmospheric ammonia over the world's major agricultural areas detected from space. *Geophys Res Lett* 44:2875–2884.
5. Georgii HW, Müller WJ (1974) On the distribution of ammonia in the middle and lower troposphere. *Tellus* 26:180–184.
6. Ziereis H, Arnold F (1986) Gaseous ammonia and ammonium ions in the free troposphere. *Nature* 321:503–505.
7. Erisman J-W, Vermetten AWM, Asman WAH, Waijers-Ijpelaan A, Slanina J (1988) Vertical distribution of gases and aerosols: The behaviour of ammonia and related components in the lower atmosphere. *Atmos Environ* 22:1153–1160.
8. Heald CL, et al. (2012) Atmospheric ammonia and particulate inorganic nitrogen over the United States. *Atmos Chem Phys* 12:10295–10312.
9. Höpfner M, et al. (2016) First detection of ammonia (NH3) in the Asian summer monsoon upper troposphere. *Atmos Chem Phys* 16:14357–14369.
10. Froyd KD, et al. (2009) Aerosol composition of the tropical upper troposphere. *Atmos Chem Phys* 9:4363–4385.
11. Wang J, Hoffmann AA, Park RJ, Jacob DJ, Martin ST (2008) Global distribution of solid and aqueous sulfate aerosols: Effect of the hysteresis of particle phase transitions. *J Geophys Res* 113:D11206.
12. Jaeglé L, et al. (1997) Observations of OH and HO2 in the upper troposphere suggest a major source from convection. *Geophys Res Lett* 24:3181–3184.
13. Mari C, Jacob DJ, Bechtold P (2000) Transport and scavenging of soluble gases in a deep convective cloud. *J Geophys Res* 105:22255–22267.
14. Liu C, Zipser EJ (2005) Global distribution of convection penetrating the tropical tropopause. *J Geophys Res* 110:D23104.
15. Danielsen EF (1993) In situ evidence of rapid, vertical, irreversible transport of lower tropospheric air into the lower tropical stratosphere by convective cloud turrets and by larger-scale upwelling in tropical cyclones. *J Geophys Res* 98:8665–8681.
16. Kritz MA, Rosner SW, Kelly KK, Loewenstein M, Chan KR (1993) Radon measurements in the lower tropical stratosphere: Evidence for rapid vertical transport and dehydration of tropospheric air. *J Geophys Res* 98:8725–8736.
17. Kelly K, et al. (1993) Water vapor and cloud water measurements over Darwin during the STEP 1987 tropical mission. *J Geophys Res* 98:8713–8723.
18. Pfister L, et al. (1993) Gravity waves generated by a tropical cyclone during the STEP tropical field program–A case study. *J Geophys Res* 98:8611–8638.
19. Vernier JP, Thomason L, Kar J (2011) CALIPSO detection of an Asian tropopause aerosol layer. *Geophys Res Lett* 38:L07804.
20. Paulot F, et al. (2014) Ammonia emissions in the United States, European Union, and China derived by high-resolution inversion of ammonium wet deposition data: Interpretation with a new agricultural emissions inventory (MASAGE_NH3). *J Geophys Res* 119:4343–4364.
21. Van Damme M, et al. (2015) Worldwide spatiotemporal atmospheric ammonia (NH_3) columns variability revealed by satellite. *Geophys Res Lett* 42:8660–8668.
22. von Bobrutzki K, et al. (2010) Field inter-comparison of eleven atmospheric ammonia measurement techniques. *Atmos Meas Tech* 3:91–112.
23. Beer R, et al. (2008) First satellite observations of lower tropospheric ammonia and methanol. *Geophys Res Lett* 35:L09801.
24. Coheur P-F, Clarisse L, Turquety S, Hurtmans D, Clerbaux C (2009) IASI measurements of reactive trace species in biomass burning plumes. *Atmos Chem Phys* 9:5655–5667.
25. Shephard MW, Cady-Pereira KE (2015) Cross-track Infrared Sounder (CrIS) satellite observations of tropospheric ammonia. *Atmos Meas Tech* 8:1323–1336.
26. Dammers E, et al. (2015) Retrieval of ammonia from ground-based FTIR solar spectra. *Atmos Chem Phys* 15:12789–12803.
27. Clarisse L, et al. (2010) Satellite monitoring of ammonia: A case study of the San Joaquin Valley. *J Geophys Res* 115:D13302.
28. Oelhaf H, Leupolt A, Fischer H (1983) Discrepancies between balloon-borne IR atmospheric spectra and corresponding synthetic spectra calculated line by line around 825 cm^{-1}. *Appl Opt* 22:647–649.
29. Coheur P-F, et al. (2007) ACE-FTS observation of a young biomass burning plume: First reported measurements of C_2H_4, C_3H_6O, H_2CO and PAN by infrared occultation from space. *Atmos Chem Phys* 7:5437–5446.
30. Burgess A, Dudhia A, Grainger R, Stevenson D (2006) Progress in tropospheric ammonia retrieval from the MIPAS satellite instrument. *Adv Space Res* 37:2218–2221.
31. Blohn V (2013) The retention of ammonia and sulfur dioxide during riming of ice particles and dendritic snow flakes: Laboratory experiments in the Mainz vertical wind tunnel. *J Atmos Chem* 70:131–150.
32. Voisin D, Legrand M, Chaumerliac N (2000) Scavenging of acidic gases (HCOOH, CH_3COOH, HNO_3, HCl, and SO_2) and ammonia in mixed liquid-solid water clouds at the Puy de Dôme mountain (France). *J Geophys Res* 105:6817–6835.
33. Lamb D, Blumenstein R (1987) Measurement of the entrapment of sulfur dioxide by rime ice. *Atmos Environ* 21:1765–1772.
34. Iribarne J, Pyshnov T (1990) The effect of freezing on the composition of supercooled droplets—I. Retention of HCl, HNO_3, NH_3 and H_2O_2. *Atmos Environ Part A Gen Top* 24:383–387.
35. Iribarne J, Barrie L, Iribarne A (1983) Effect of freezing on sulfur dioxide dissolved in supercooled droplets. *Atmos Environ* 17:1047–1050.
36. Stuart A, Jacobson M (2004) Chemical retention during dry growth riming. *J Geophys Res* 109:D07305.
37. Leriche M, Pinty J, Mari C, Gazen D (2013) A cloud chemistry module for the 3-D cloud-resolving mesoscale model Meso-NH with application to idealized cases. *Geosci Model Dev* 6:1275–1298.
38. Hoog I, Mitra SK, Diehl K, Borrmann S (2007) Laboratory studies about the interaction of ammonia with ice crystals at temperatures between 0 and –20°C. *J Atmos Chem* 57:73–84.
39. Pruppacher HR, Klett JD (2012) *Microphysics of Clouds and Precipitation: Reprinted 1980* (Springer, Dordrecht, The Netherlands).
40. Vučković V, Vujović D (2017) The effect of mass transfer parameterization and ice retention on the scavenging and redistribution of SO_2 by a deep convective cloud. *Environ Sci Pollut Res Int* 24:3970–3984.
41. Salzmann M, Lawrence M, Phillips V, Donner L (2007) Model sensitivity studies regarding the role of the retention coefficient for the scavenging and redistribution of highly soluble trace gases by deep convective cloud systems. *Atmos Chem Phys* 7:2027–2045.
42. Snider JR, Huang J (1998) Factors influencing the retention of hydrogen peroxide and molecular oxygen in rime ice. *J Geophys Res* 103:1405–1415.
43. Michael R, Stuart AL (2009) The fate of volatile chemicals during wet growth of a hailstone. *Environ Res Lett* 4:015001.
44. Ervens B (2015) Modeling the processing of aerosol and trace gases in clouds and fogs. *Chem Rev* 115:4157–4198.
45. Wang J, Jacob DJ, Martin ST (2008) Sensitivity of sulfate direct climate forcing to the hysteresis of particle phase transitions. *J Geophys Res* 113:D11207.
46. Streets D, Yarber K, Woo JH, Carmichael G (2003) Biomass burning in Asia: Annual and seasonal estimates and atmospheric emissions. *Global Biogeochem Cycles* 17:1099.
47. Huang X, et al. (2012) A high-resolution ammonia emission inventory in China. *Global Biogeochem Cycles* 26:GB1030.
48. Huang L, Jiang JH, Murray LT, Damon MR, Livesey NJ (2016) Evaluation of UTLS carbon monoxide simulations in GMI and GEOS-Chem chemical transport models using Aura MLS observations. *Atmos Chem Phys* 16:5641–5663.
49. Zhang L, et al. (2012) Nitrogen deposition to the United States: Distribution, sources, and processes. *Atmos Chem Phys* 12:4539–4554.
50. Liu H, Jacob DJ, Bey I, Yantosca RM (2001) Constraints from ^{210}Pb and ^{7}Be on wet deposition and transport in a global three-dimensional chemical tracer model driven by assimilated meteorological fields. *J Geophys Res* 106:12109–12128.
51. Heymsfield AJ, Bansemer A, Heymsfield G, Fierro AO (2009) Microphysics of maritime tropical convective updrafts at temperatures from –20 to –60. *J Atmos Sci* 66:3530–3562.
52. Koop T, Luo B, Tsias A, Peter T (2000) Water activity as the determinant for homogeneous ice nucleation in aqueous solutions. *Nature* 406:611–614.
53. Kremser S, et al. (2016) Stratospheric aerosol—Observations, processes, and impact on climate. *Rev Geophys* 54:278–335.
54. Kravitz B, Robock A, Oman L, Stenchikov G, Marquardt AB (2009) Sulfuric acid deposition from stratospheric geoengineering with sulfate aerosols. *J Geophys Res* 114:D14109.
55. Bigg E (1976) Size distributions of stratospheric aerosols and their variations with altitude and time. *J Atmos Sci* 33:1080–1086.
56. Gras J (1978) Change in nature of stratospheric aerosol collected at 34°S. *Nature* 271:231–232.
57. Turco R, Whitten R, Toon O (1982) Stratospheric aerosols: Observation and theory. *Rev Geophys* 20:233–279.
58. Abbatt JP, et al. (2006) Solid ammonium sulfate aerosols as ice nuclei: A pathway for cirrus cloud formation. *Science* 313:1770–1773.
59. Bey I, et al. (2001) Global modeling of tropospheric chemistry with assimilated meteorology: Model description and evaluation. *J Geophys Res* 106:23073–23095.